Complex energy shift and background phase shift for simulated electron-molecular shape resonances

G. A. Gallup*
Department of Physics and Astronomy, University of Nebraska–Lincoln, Lincoln, Nebraska 68588-0111, USA
(Received 19 August 2004; published 17 February 2005)

Feshbach-Fano resonance theory (FFRT) is used to determine the energy dependence of the complex energy shift function, consisting of the real energy shift and the resonance width, and the background phase shift for several simulated molecular shape resonances. Attention is paid to the way the choice of the quasibound state (QBS) function required in the FFRT affects these energy dependencies. An overlap criterion for choosing an optimal QBS function is proposed. Using our treatment on *t*-butylchloride, carbon tetrachloride, ethylene, and benzene, we give numerical results for specific cases of $l=1$ through 4. We find that the real energy shift function does not vary greatly over the width of the resonance, although the magnitude of the shift can be fairly large. We also find that the behavior of the background phase shift due to orthogonality scattering is sensitive to the presence of long-range potentials.

DOI: 10.1103/PhysRevA.71.022710 PACS number(s): 34.80.Bm, 34.80.Ht, 34.80.Gs

I. INTRODUCTION

When low-energy electrons impinge on molecules, the two most important inelastic processes are vibrational excitation (VE) and dissociative electron attachment (DEA). Both of these involve transfer of electron kinetic energy to the nuclei and, because of the disparate masses of electrons and nuclei, such transfer was traditionally expected to be small. Nevertheless, it does occur with considerable probability because of resonant processes due to the potential energy of interaction between the electron and the molecule. Core excited resonances also occur and can produce VE and DEA, but these tend to appear at higher energies, and except for one instance we restrict the discussion in this article to the shape resonance regime.

The discussion of nuclear motion in molecules typically uses the Born-Oppenheimer or adiabatic approximation to separate electronic and nuclear motion and to relate the electronic energy at fixed nuclear positions to the nuclear potential energy. When dealing with resonances, the electronic state is decaying with a certain lifetime, and the resulting nuclear potential energy function is nonlocal and complex. Most treatments of these resonances have used the Feshbach-Fano resonance procedure (FFRP) [1–4], which results in a lifetime and an energy shift that are functions of the nuclear coordinates and the total energy of the wave function. These quantities are important parts of the nonlocal complex potential the nuclei react to, and it is the principal purpose of this article to analyze the exact scattering solutions for simulated potentials to gain further insight into how lifetimes and energy shifts vary with energy at a given nuclear geometry. Thus, in this article we focus on the behavior of the electronic parts of the theory and do not directly address matters of nuclear dynamics.

The FFRP must start with a choice for an approximate representation of the inner part of the continuum wave function at energies near the resonance. This function, which must be square-integrable, is usually viewed as representing a quasibound state (QBS) embedded in the continuum. The principal difficulty arises because there is no clear-cut criterion for choosing this QBS function. Although exact results must be independent of the choice, real calculations with approximations are usually not so fortunate, and one of our goals here is to examine how the normal approximations that must be made in any practical calculation affect the results and their likely differences from exact answers. This requires exact results, and to facilitate obtaining such, we use spherical piecewise constant potentials. Although real molecules never have spherically symmetric potentials, experiment shows there are cases when resonance states are sufficiently closely approximated by a single l wave that our calculations can give a useful picture of their behavior.

Our potentials should have some similarity to real systems, and we use a potential with an arbitrary number of segments [5]. In this way, the effects of long-range forces may be included up to the limitations of the approximations. Such piecewise spherical potentials may always be solved analytically and the wave functions written in a finite number of terms. Nevertheless, for a potential of any considerable number of segments, such expressions would have little practical utility. Therefore, most of our examples are worked out and displayed in numerical form only. The exception is the study on the plane wave where the relatively simple form of the analytical expressions has considerable informational content.

Resonant behavior of square-well potentials has been studied before [6–10], with much of the emphasis on the behavior of *S*-matrix poles. Our goal, however, is somewhat different—we are particularly interested in how the choice of the quasibound resonant state affects the results of the calculation. For this reason, unlike some earlier studies, we focus on states of $l>0$ where shape resonances produced by centrifugal barriers occur.

*Electronic address: ggallup@unlserve.unl.edu; URL: http://physics.unl.edu/~ggallup/gallup.html

II. THEORY

The FFRP has been described by a number of workers in various forms [1–4,10–12], and although the details differ somewhat, the basic theory is the same. It is assumed that the system has a resonance that may be viewed as a QBS *embedded in the continuum*. The inner part of the wave function at energies near resonance, the QBS function itself, is symbolized by $|q\rangle$ and is assumed normalizable. Separate from this and orthogonal to it, we have the background continuum function, $\phi^{(b)}_{E\hat{k}}$. These functions have the properties

$$\langle q|q\rangle = 1, \tag{1}$$

$$\langle q|\phi^{(b)}_{E\hat{k}}\rangle = 0, \tag{2}$$

$$\langle \phi^{(b)}_{E'\hat{k}'}|\phi^{(b)}_{E\hat{k}}\rangle = \delta(E'-E)\,\delta(\hat{k}'-\hat{k}). \tag{3}$$

The matrix elements of the Hamiltonian for this basis are assumed to take the form

$$\langle q|H|q\rangle = E_q, \tag{4}$$

$$\langle q|H|\phi^{(b)}_{E\hat{k}}\rangle = V_{E\hat{k}}, \tag{5}$$

$$\langle \phi^{(b)}_{E'\hat{k}'}|H|\phi^{(b)}_{E\hat{k}}\rangle = E\,\delta(E'-E)\,\delta(\hat{k}'-\hat{k}). \tag{6}$$

Of course, Eq. (6) does not imply that $\phi^{(b)}_{E\hat{k}}$ is an eigenfunction of H. Rather, because of Eqs. (2) and (5), we have

$$(H-E)\phi^{(b)}_{E\hat{k}} = V_{E\hat{k}}|q\rangle. \tag{7}$$

Thus, $\phi^{(b)}_{E\hat{k}}$ is a solution of an inhomogeneous Schrödinger equation. We now let $G^a(\vec{r}',\vec{r})=(H-E)^{-1}$ be the Green's function with some specified asymptotic behavior, and the function $\phi^{(b)}_{E\hat{k}}$ may be written

$$\phi^{(b)}_{E\hat{k}} = N\left[\phi^{(h)}_{E\hat{k}} - G^a|q\rangle\frac{\langle q|\phi^{(h)}_{E\hat{k}}\rangle}{\langle q|G^a|q\rangle}\right], \tag{8}$$

where $\phi^{(h)}_{E\hat{k}}$ is a solution to the homogeneous Schrödinger equation, and N must be adjusted so that Eq. (3) is satisfied, which requires that $N=\cos\delta^{(b)}$. This phase shift will be defined below. Equation (2) is clearly satisfied by the solution of Eq. (8). If we introduce the projection operators P and Q such that $P+Q=I$ and $Q=|q\rangle\langle q|$, one sees that

$$P(H-E)P\phi^{(b)}_{E\hat{k}} = 0, \tag{9}$$

and it is a solution to the Schrödinger equation projected onto the P space.

We do not use the full three-dimensional $E\hat{k}$ designations in our considerations, since the actual potentials in the Hamiltonians are spherical. Thus, an lm basis version of Eqs. (1)–(8) is used, and we may work within an individual l subspace. Asymptotically, in this representation we have

$$\phi^{(h)}_l \to \sin(\varphi_l + \delta^{(h)}), \tag{10}$$

$$\phi^{(b)}_l \to \sin(\varphi_l + \delta^{(b)}), \tag{11}$$

$$\varphi_l = kr - \pi l/2, \tag{12}$$

where $(\delta^{(h)})$ and $(\delta^{(b)})$ are the phase shifts for the homogeneous and the background equations, respectively. $\delta^{(h)}$ is the total phase shift for the problem, of course. One sees here the incongruous situation in which we find ourselves. In order to formulate the problem of the nuclear motion in the Born-Oppenheimer or adiabatic approximations, we need to express the electronic wave function in a resonance form. Separating the description into resonance and background parts requires us to solve the exact problem in the first place. Nevertheless, the direct use of the $\phi^{(h)}_l$ matrix elements in the nuclear problem appears difficult. Of course, if one is planning an approximate partly phenomenological treatment, some of the quantities will be obtained using physical arguments, and an exact solution is skirted.

The primary result of FFRP gives formulas for the width and energy shift of the resonance. The width function $\Gamma(E)$ is given by

$$\Gamma_l(E) = \frac{4}{k}|\langle q|H|\phi^{(b)}_l\rangle|^2, \tag{13}$$

and the energy shift function is

$$\Delta_l(E) = \frac{1}{2\pi}\int_0^\infty \frac{\Gamma_l(E')dE'}{E-E'}. \tag{14}$$

In terms of these quantities, the resonant phase shift is

$$\tan(\delta^{(res)}_l) = -\frac{\Gamma_l(E)/2}{E-E_q-\Delta_l(E)}, \tag{15}$$

where $E_q=\langle q|H|q\rangle$ is the eigenvalue of the Hamiltonian in the Q subspace. These results also imply

$$\delta^{(h)}_l = \delta^{(b)}_l + \delta^{(res)}_l. \tag{16}$$

III. CALCULATIONAL PROCEDURE

A. General considerations

Domcke [10] has suggested a specific three-step procedure, practical with realistic systems, for applying the FFRP to shape resonances in molecules. We show a "flow chart" that contains his recommended steps.

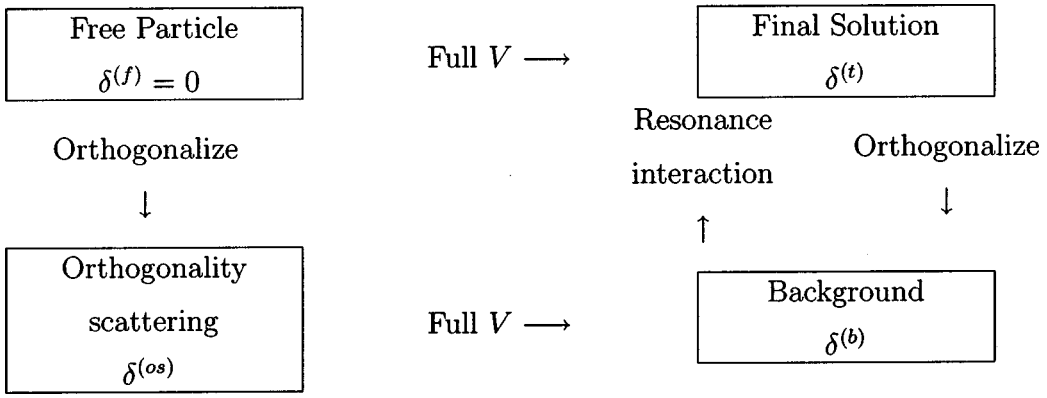

We label the stages in the diagram with a symbol for the phase shift that exists at that point.

(i) $\delta^{(f)}$: This represents the free particle, which has no phase shift (from itself).

(ii) $\delta^{(t)}$: This represents the final solution, which has the actual total phase shift. This is directly obtained from the solution of the Schrödinger equation with the potential V.

(iii) $\delta^{(os)}$: This represents the free continuum orthogonalized to the QBS function chosen to represent the resonance. This has been called the orthogonality scattering phase shift.

(iv) $\delta^{(b)}$: This represents the background solution obtained by solving the Schrödinger equation with the potential V under the orthogonality constraint.

Using these symbols, Domcke's suggestion is

$$\delta^{(f)} \rightarrow \delta^{(os)} \rightarrow \delta^{(b)} \rightarrow \delta^{(t)},$$

going around the bottom of the diagram. The reader is referred to Domcke's discussion for a rationale to justify this apparently roundabout procedure.

Since we consider single-particle potential scattering systems in this article, a slightly less circuitous process is simpler. This is represented by the extra $\downarrow$ step added to the right column of the flow chart. Thus, since our goal is to examine the behavior of the exact resonance width, energy shift, and background phase-shift functions for exactly solvable potentials, we may, in principle, proceed from the final solution to the background function rather than using the opposite direction, which is Domcke's final step.

B. Present mathematical procedure

The total wave function must satisfy the l-subspace Schrödinger equation,

$$(H_l - E)\psi_l = 0, \tag{17}$$

$$H_l = -\frac{d^2}{2dr^2} + \frac{l(l+1)}{2r^2} + V(r), \tag{18}$$

and to carry out the separation we will need the Green's function associated with Eq. (17) from which we obtain the regular solution. We also need the irregular solution, which we denote ζ_l. These are arranged to have the asymptotic behaviors

$$\psi_l \rightarrow \sin(\varphi_l + \delta_l^{(t)}), \tag{19}$$

$$\zeta_l \rightarrow -\cos(\varphi_l + \delta_l^{(t)}), \tag{20}$$

where

$$\varphi_l = kr - \frac{\pi l}{2}.$$

$\delta_l^{(t)}$ in these is the total phase shift in channel l for our system. It is this quantity that we will be partitioning into a background and resonant part. In terms of these solutions, the standing-wave Green's function is

$$G_t^0(r,r') = -\frac{2}{k}\psi_l(r_<)\zeta_l(r_>). \tag{21}$$

As we shall see, once the specific form of the QBS function is chosen, the width, energy shift, and background phase-shift functions may all be written quite simply in terms of the matrix element of this Green's function $\langle q_l|G_t^0|q_l\rangle$ and the overlap $\langle q_l|\psi_l\rangle$.

We need now to orthogonalize the total solution to the QBS function. The usual way to orthogonalize an arbitrary function, ϕ, to a given one is to use the Schmidt procedure, yielding $\phi - q_l\langle q_l|\phi\rangle$ for a result. We must do this so that our function is also a solution of

$$P(H_l - E)P\phi = 0, \tag{22}$$

$$P = I - |q_l\rangle\langle q_l|, \tag{23}$$

and one accomplishes this with a simple generalization of the Schmidt procedure. Considering any third function, g, linearly independent of ϕ, we see that

TABLE I. Roots of j_l Riccati-Bessel functions.

Root	j_1	j_2	j_3	j_4
1	4.49340946	5.76345920	6.98793200	8.18256145
2	7.72525184	9.09501133	10.41711855	11.70490715

$$\phi - g\frac{\langle q_l|\phi\rangle}{\langle g|q_l\rangle}$$

is properly orthogonal to q_l. The Schmidt result occurs when $g=q_l$. We satisfy both of our requirements by using G_t^0 to construct g, and the result is

$$\phi = N_\phi\left[\psi_l - G_t^0|q_l\rangle\frac{\langle q_l|\psi_l\rangle}{\langle q_l|G_t^0|q_l\rangle}\right], \tag{24}$$

where N_ϕ is a normalization constant defined below.

From the definition of G_t^0, we see that

$$G_t^0|q_l\rangle \to -\frac{2}{k}\zeta_l\langle\psi_l|q_l\rangle \tag{25}$$

for large r, and

$$\phi \to N_\phi[\sin(\varphi_l + \delta_l^{(t)}) - K\cos(\varphi_l + \delta_l^{(t)})], \tag{26}$$

$$K = \frac{2\langle\psi_l|q_l\rangle^2}{k\langle q_l|G_t^0|q_l\rangle}, \tag{27}$$

$$N_\phi = (1+K^2)^{-1/2}, \tag{28}$$

where K is the tangent of the angle that when subtracted from $\delta^{(t)}$ gives $\delta^{(b)}$. Therefore,

$$\tan\delta_l^{(res)} = K, \tag{29}$$

$$= \frac{2\langle\psi_l|q_l\rangle^2}{k\langle q_l|G_t^0|q_l\rangle}, \tag{30}$$

$$N_\phi = \cos\delta_l^{(res)}. \tag{31}$$

According to the usual prescriptions of the FFRP, one has

$$\Gamma(E) = 2\pi|V_k|^2, \tag{32}$$

$$V_k = \sqrt{\frac{2}{\pi k}}\langle q_l|H_l|\phi\rangle, \tag{33}$$

where $\sqrt{(2/\pi k)}$ is the factor required to "energy-normalize" the function, ϕ. Because of the orthogonality,

$$\langle q_l|H_l|\phi\rangle = \langle q_l|H_l - E|\phi\rangle, \tag{34}$$

$$= -\frac{\langle q_l|\psi_l\rangle N_\phi}{\langle q_l|G_t^0|q_l\rangle}, \tag{35}$$

$$\Gamma(E) = \frac{4}{k}\left(\frac{\langle q_l|\psi_l\rangle N_\phi}{\langle q_l|G_t^0|q_l\rangle}\right)^2. \tag{36}$$

Furthermore, the well known formula for the resonant phase shift is

$$\tan\delta_l^{(res)} = -\frac{\Gamma(E)/2}{E - E_q - \Delta(E)}, \tag{37}$$

and combining all of these results allows us to calculate the energy shift simply as

$$\Delta(E) = E - E_q + \frac{\cos^2\delta_l^{(res)}}{\langle q_l|G_t^0|q_l\rangle}. \tag{38}$$

Berman *et al.* [13] have emphasized the importance and convenience of determining $\Delta(E)$ without using a formula like that of Eq. (14), which requires a knowledge of $\Gamma(E)$ up to high enough energies to converge. Our result has the same convenience.

The peak of the resonance part of the cross section is near an energy, E_{res}, when $\delta_l^{(res)} = \pi/2$, i.e., E_{res} is the root of the equation

$$E_{res} - E_q - \Delta(E_{res}) = 0, \tag{39}$$

and this root must be a simple zero. Using Eqs. (38) and (39), we see that

$$\left.\frac{\cos^2\delta_l^{(res)}}{\langle q_l|G_t^0|q_l\rangle}\right|_{E_{res}} = 0 \tag{40}$$

also. The numerator of this fraction has a quadratic zero at E_{res}, therefore the denominator must have a simple zero at this energy, and we have the interesting result that

$$\langle q_l|G_t^0(E_{res})|q_l\rangle = 0, \tag{41}$$

which we discuss further in Sec. VI.

IV. THE QUASIBOUND STATE FUNCTIONS

For the segmented piecewise constant potentials we treat, it is natural to follow earlier workers and, for the $|q\rangle$ functions, use Riccati-Bessel functions truncated at one of the zeros. Table I gives the first two roots of the regular functions for $l=1$ to 4. Thus, if $j_l(\eta_{ln})=0$, $\eta_{ln}>0$ is the nth root corresponding to the function of order l.

Perhaps a word of caution is called for here. QBS functions of this sort are L^2, but have a discontinuous first derivative, and the kinetic energy operator is not Hermitian in mixed integrals between these and continuum functions. For complete rigor, the function with the discontinuous first derivative must be treated as the limit of one with an increas-

ingly sharp exponential fall-off. The kinetic energy operator then behaves correctly.

V. MODEL CALCULATIONS

The first system we treat is one with no potential, i.e., a free l wave. Considering the flow diagram, for this case $V=0$, and the two columns represent the same pair of systems. Our example here is thus equivalent to the initial step in Domcke's procedure [10] of using orthogonalized plane waves as the starting point of the FFRP treatment of more complicated systems. He has illustrated this with an s-wave example. We give results for a general l value.

In addition to the treatment of the free particle, we show results from calculations of several simple well and segmented potentials. These include (i) a resonance analysis of a simple well parametrized to match the properties of a C—Cl σ^* p-wave resonance, (ii) a resonance analysis of a segmented potential parametrized to duplicate the properties of the $^2T_2$ p-wave resonance in CCl_4, (iii) a resonance analysis of a segmented potential parametrized to duplicate the properties of the $^2B_{2g}$ d-wave resonance in C_2H_4, and (iv) a resonance analysis of segmented potentials parametrized to duplicate the properties in C_6H_6 of both the $^2E_{2u}$ f-wave resonance and the hypothetical shape part of the $^2B_{2g}$ g-wave resonance. The details of the potentials will be given with each example.

We emphasize that the calculations we describe are made with spherical potentials, and the states in such systems have an actual degeneracy of $2l+1$. Nevertheless, when we associate a system with an actual molecule, we use the correct degeneracy of the molecular state when giving results that depend upon that quantity. This refers principally to graphs of cross sections in the following.

A. The FFRP applied to a free particle

As described in Sec. IV, the Q space is based upon the function

$$q_l(r) = N_l j_l(\alpha r), \quad r < r_0, \tag{42}$$

$$= 0; r_0 < r, \tag{43}$$

$$\alpha = \eta_{l1}/r_0, \tag{44}$$

$$N_l = \sqrt{\frac{2}{r_0}} y_l(\alpha r_0), \tag{45}$$

where r_0 is the radius of the $|q\rangle$ function. There is, of course, no reason inherent in this system for choosing a particular value of r_0. Our Hamiltonian is simply

$$H = H_l = -\frac{d^2}{2dr^2} + \frac{l(l+1)}{2r^2}. \tag{46}$$

It is now a straightforward calculation to determine the background function from Eq. (8). We use the standing-wave Green's function

$$G^0 = -\frac{2}{k} j_l(kr_<) y_l(kr_>), \tag{47}$$

where the asymptotic specifications for j_l and y_l are those of Abramowitz and Stegun [14]. All of the integrations are familiar, being of Bessel function products. One obtains

$$\langle q_l | j_l \rangle = -\sqrt{\frac{2}{r_0}} \frac{\alpha j_l(\beta)}{\alpha^2 - k^2}, \tag{48}$$

$$\langle q_l | G^0 | q_l \rangle = \frac{2}{\alpha^2 - k^2} - \frac{4\alpha^2 j_l(\beta) y_l(\beta)}{\beta(\alpha^2 - k^2)^2}, \tag{49}$$

$$G^0 | q_l \rangle \to -2 \langle q_l | j_l \rangle y_l(kr)/k, \tag{50}$$

where $\beta = kr_0$. We also note that the matrix element, $\langle q_l | G^0 | q_l \rangle$, given by Eq. (49) is not singular at $k=\alpha$, but rather

$$\lim_{k\to\alpha} \langle q_l | G^0 | q_l \rangle = -\frac{3 + 2\alpha r_0 j_l'(\alpha r_0) y_l'(\alpha r_0)}{2\alpha^2},$$

where j_l' and y_l' are the derivative functions corresponding to the Bessel functions.

After some simplification, one obtains

$$\tan \delta^{(b)} = \frac{\alpha^2 j_l(\beta)^2/\beta}{k^2/2 - \alpha^2/2 + \alpha^2 j_l(\beta) y_l(\beta)/\beta}, \tag{51}$$

which agrees with Domcke's result for the case $l=0$ and a Q space of one function. Since the result of the resonance treatment must be to return the phase shift to zero, we obviously have $\delta^{(res)} = -\delta^{(b)}$.

The threshold law for $\delta^{(b)}$ is

$$\delta^{(b)} \approx -\frac{2\beta^{2l+1}}{(2l-1)!!(2l+3)!!}, \tag{52}$$

and $\tan \delta^{(b)} \to 0$ as $E \to \infty$. Thus, depending upon the quadrant we assume for the arctangent function, $\delta^{(b)}$ varies from 0 to $-\pi$ or from π to 0. Previous workers have usually chosen the former alternative for the background phase shift. The rate at which $\delta^{(b)}$ approaches $-\pi$ varies with r_0 as predicted by Wigner's result [15], limiting the derivative of the phase shift with respect to k to values $> -r_0$. Figure 1 shows this for four cases and $l=1$.

We now change notation slightly and use $\phi_l^{(b)}$ for our normalized background function corresponding to l, and we now find that the resonance width for this system is[1]

$$\Gamma(E) = \frac{4}{k} |\langle q_l | H_l | \phi_l^{(b)} \rangle|^2, \tag{53}$$

$$= \frac{4 \cos^2 \delta^{(b)} \langle q_l | j_l \rangle^2}{k \langle q_l | G^0 | q_l \rangle^2}. \tag{54}$$

Finally, using Eq. (38) we obtain

[1]Here is where the non-Hermitian problem of the Hamiltonian arises for the b functions used. It will be seen that $\langle \phi_l^{(b)} | H_l | b \rangle = 0$ if evaluated directly since $H_l|b\rangle$ is proportional to $|b\rangle$.

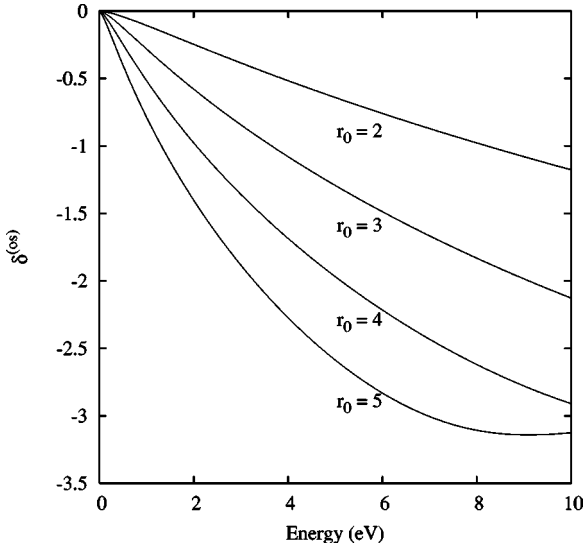

FIG. 1. The variation of $\delta^{(b)}$ with energy for a free electron for four values of r_0 (in Å) and for $l=1$.

$$\Delta(E) = E - E_q + \frac{\cos^2 \delta^{(b)}}{\langle q_l | G^0 | q_l \rangle}. \tag{55}$$

Figure 2 shows how several of these quantities vary with electron energy for the special case of $r_0=3$ Å and $l=1$. It may be noted in particular that $\langle q_l|G^0|q_l\rangle$ has one simple zero in the range of the graph. This is in line with the discussion leading up to Eq. (41). We will discuss these results further in Sec. VI after we have examined systems with potentials that support centrifugal barrier shape resonances.

B. Influence of well size on dip-to-peak separation

Most of the measurements of molecular resonances have, because of its sensitivity, used the electron transmission spectroscopy (ETS) method [16], which yields the negative of the first derivative of the total cross section with respect to energy. The presence of a resonant peak in the total cross section gives a signature structure in the electron transmission spectrum consisting of a dip followed by a peak with increasing energy. Since one is determining the derivative of the cross section, dip and peak extrema correspond to inflection points. The experimental quantity of interest here is the dip-to-peak energy separation, since, in simple cases, it is closely related to the lifetime of the resonance.[2] In our work, however, we determine the resonance cross section and differentiate it to obtain the derivative curve and the dip-to-peak separation directly.

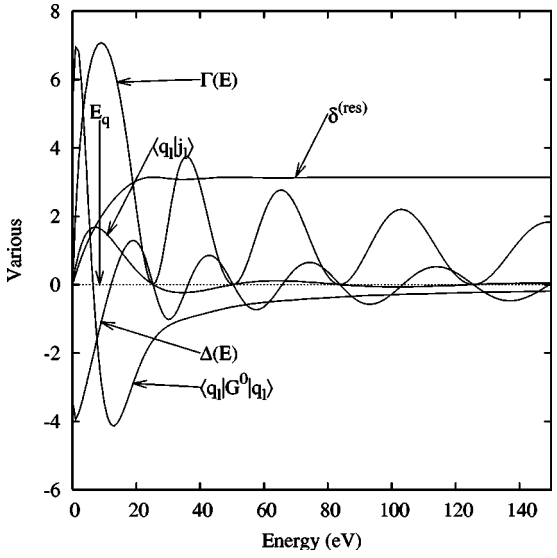

FIG. 2. The graphs of several integrals, matrix elements, or phase shifts for $r_0=3$ Å and $l=1$ for a free electron. The energies are all in eV, the phase shift is in radians, and the others are in a.u. Only $\delta^{(res)}$ is shown since $\delta^{(b)}$ is its negative. E_q is also shown by a vertical arrow.

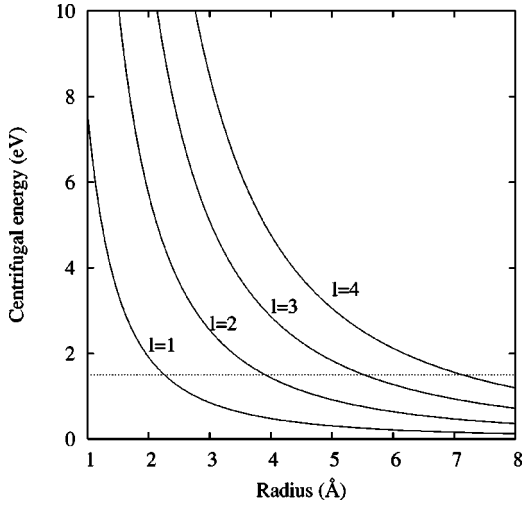

FIG. 3. The centrifugal potential for l values 1 to 4. The horizontal dotted line is placed at 1.5 eV, and wells with radii outside each crossing point will not have barriers above the "resonance energy."

Before starting to examine cases with particular parameters, we wish to show how the radius of the well is related to the dip-to-peak distance of the resonance produced, and since the shape resonances we discuss are the result of angular momentum barriers, the height of the barrier for a given l is determined principally by the size of the system.

To show an example of the influence of this on dip-to-peak separation, we somewhat arbitrarily choose an energy of 1.5 eV (this is reasonably typical of molecular shape reso-

[2]For a narrow resonance, with essentially constant lifetime and energy shift and not overlapped by others, the Breit-Wigner single level formula may be used to represent the total cross section. Under these circumstances, the cross section σ may be written as

$$\sigma \propto \frac{(\Gamma/2)^2}{E[(E-E_0)^2 + (\Gamma/2)^2]}. \tag{56}$$

A straightforward calculation then shows that the dip and peak energies are

$$E_0 \mp \frac{\Gamma}{2\sqrt{3}} - \frac{\Gamma^2}{9E_0} + \Gamma \times O[(\Gamma/E_o)^2]. \tag{57}$$

Thus, through first order in Γ/E_0, the dip-to-peak separation is $\Gamma/\sqrt{3}$.

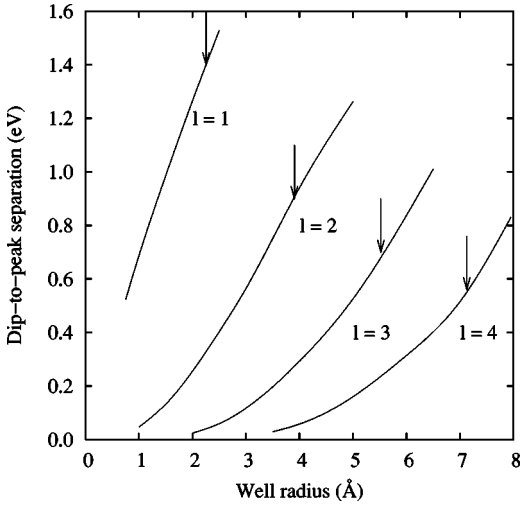

FIG. 4. The dip-to-peak separations for 1.5 eV resonance and different well radii and different l values. The arrows show the radii where the centrifugal barrier equals 1.5 eV. (see Fig. 3).

nances) and calculate the dip-to-peak energy separation as a function of the radius of the well. The depth of the well must, of course, be varied here to produce such results. Figure 3 shows graphs of the centrifugal potential for values of $l=1$ to 4 as a function of the distance from the origin. This shows that if the well radius is large enough, the centrifugal barrier height is less that our chosen resonance position.

The results are shown in Fig. 4, and one sees that the width of the resonance peak, as measured by its dip-to-peak separation, shows the expected behavior as the barrier height decreases. We also see that this measure of the width continues to increase smoothly for a short distance above the barrier, at least. The arrows in Fig. 4 show the radii at which each barrier is 1.5 eV.

The most noteworthy aspect of the results shown in Fig. 4 is that the dip-to-peak energy separation behaves qualitatively just as the threshold behavior of the spherical Bessel function that is the inner portion of the solution for each l, i.e., r^l.

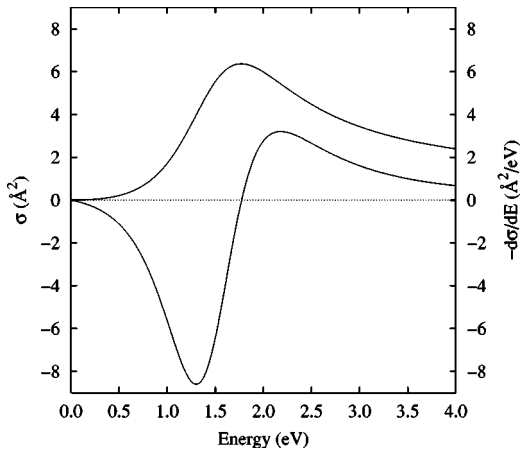

FIG. 5. The cross section and the negative of its derivative with respect to energy for the C—Cl σ^* orbital of $(CH_3)_3CCl$ and $l=1$.

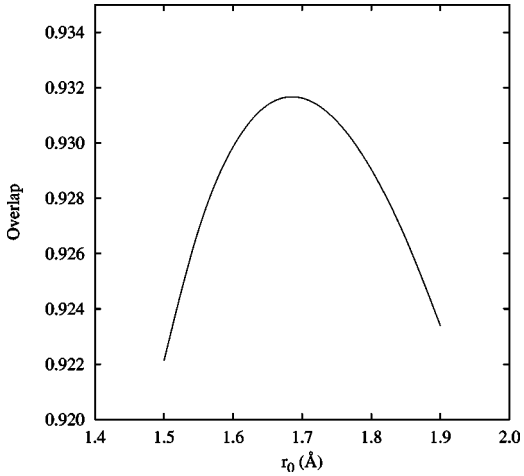

FIG. 6. The overlap (squared) criterion for the "best" QBS function plotted vs r_0 for $(CH_3)_3CCl$ and $l=1$.

C. An overlap criterion for choosing the QBS function

We now examine a simple square well and include selected results of several calculations. As mentioned above, one of our goals is to investigate how one might determine when a particular QBS function is optimal for the situation at hand. An intuitive criterion is to require a function that matches most closely the inner part of the wave function at an energy close to the cross-section peak, and we implement this in the following way.

If we have a test function $|t\rangle$, an unknown function $|x\rangle$, and both are L^2 functions normalized to 1, calculating the overlap provides a simple test for how close they are to being equal. That is, $|t\rangle=|x\rangle$ if and only if $\langle t|x\rangle=1$. Our problem is slightly more complicated in that one of our functions, ψ_l, is not L^2. Therefore, we proceed slightly differently.

Let $w(r)$ be a weight function that guarantees the convergence of our integral, and define the weighted mean-square difference between the two functions as

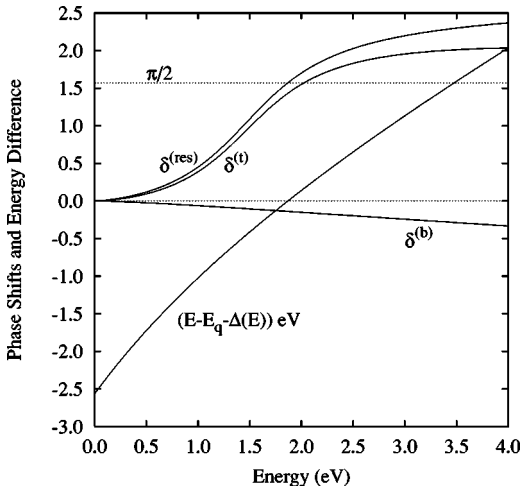

FIG. 7. The three phase shifts $\delta^{(res)}$, $\delta^{(t)}$, and $\delta^{(b)}$ vs energy for the simple potential for $(CH_3)_3CCl$. In order to guide the eye, a dotted line at $\pi/2$ is drawn across the graph. In addition, $E-E_q-\Delta(E)$ is plotted, and it crosses the x axis at E_{res} where $\delta^{(res)}$ also intersects the $\pi/2$ line.

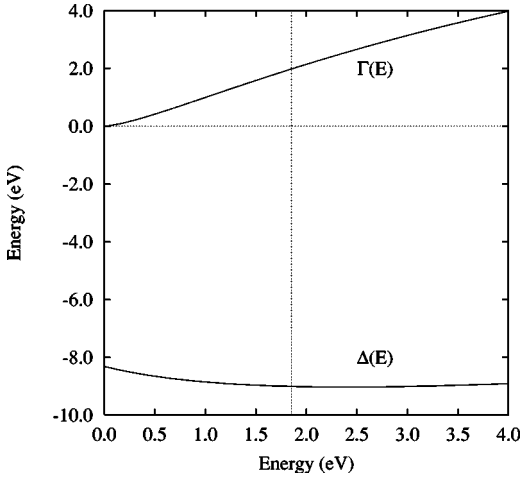

FIG. 8. The $\Gamma(E)$ and $\Delta(E)$ functions near the resonance peak for the $(CH_3)_3CCl$ potential. The vertical dotted line is added to guide the eye to the energy of the resonance maximum.

$$D = \inf\left\{ \int [b(r) - C\psi_l(r)]^2 w(r) dr \right\}, \tag{58}$$

as C is varied. It is straightforward to show that requiring D to be a minimum is equivalent to having a maximum in the quantity

$$\frac{\langle b|w|\psi_l\rangle^2}{\langle \psi_l|w|\psi_l\rangle} \leqslant \langle b|w|b\rangle. \tag{59}$$

The obviously most simple $w(r)$ function for our application is

$$w(r) = S(r_0 - r), \tag{60}$$

where $S(x)$ is the unit step function. For the truncated QBS functions, $\langle b|w|b\rangle = \langle b|b\rangle = 1$ and $\langle b|w|\psi_l\rangle = \langle b|\psi_l\rangle$. We use this criterion below.

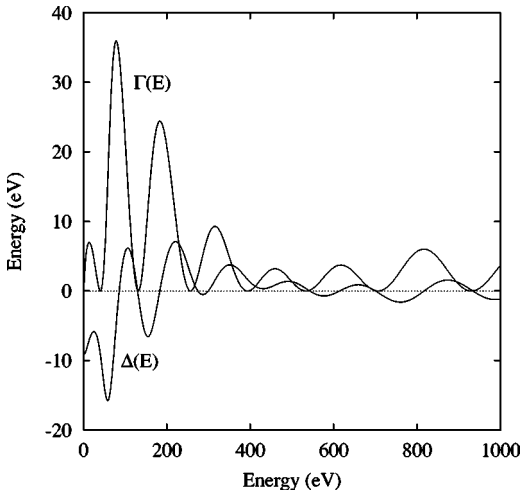

FIG. 9. $(CH_3)_3CCl$. The $\Gamma(E)$ and $\Delta(E)$ functions up to 1000 eV. Otherwise, see the caption of Fig. 8.

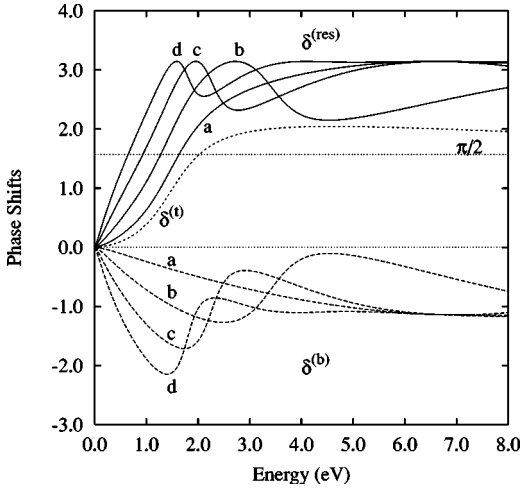

FIG. 10. The resonant and background phase shifts for the $(CH_3)_3CCl$ potential treated with a range of diffuse QBS functions. The results are for four values of r_0: *a*, 3.0; *b*, 5.0; *c*, 7.0; *d*, 9.0. All of the distances are in Å. $\delta^{(t)}$ is also shown for comparison.

D. An $l=1$ case

Some of the best examples among molecules of this case arise with the alkyl chlorides. In particular, $(CH_3)_3CCl$, *tert*-butyl chloride [17] shows a resonance in ETS around 1.86 eV. This has been assigned to the C—Cl σ^* orbital and is expected to be predominantly *p*-wave. The observed dip-to-peak separation is 1.18 eV. The C—Cl bond distance is near 1.85 Å, and in order to simulate such a situation we choose a spherical well of radius 1.0 Å, a little larger than half the actual internuclear distance. If the potential in the well is taken as -33.0 eV, we arrive at a *p*-wave resonance peak at 1.85 eV, close to the experimental value. The corresponding theoretical dip-to-peak separation of 0.89 eV in $-d\sigma/dE$ is somewhat smaller than the experimental separation. In light of the results shown in Fig. 4 and the discussion leading up to it, we would expect to be able to make the theoretical

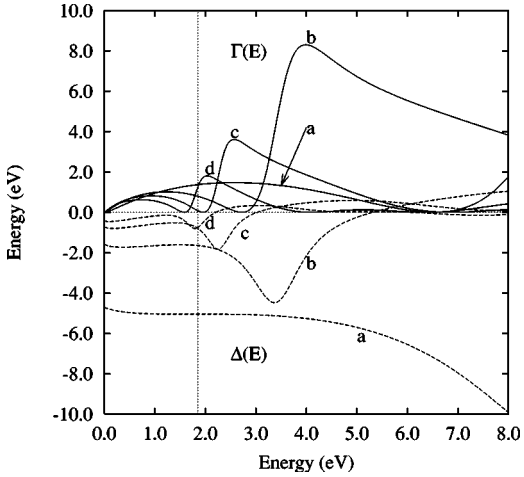

FIG. 11. The lifetimes and energy shifts for the $(CH_3)_3CCl$ potential treated with a range of diffuse QBS functions. The results are for four values of r_0: *a*, 3.0; *b*, 5.0; *c*, 7.0; *d*, 9.0. All of the distances are in Å.

TABLE II. Model potential for CCl_4.

C	bond	Cl		Polarizability tail			
0.0[a]	0.4	1.2	2.2	4.15	6.1	10.0	Å
−61.0	−35.8	−126.49	−0.27193	−0.05825	−0.00806	0.0	eV
0.4	1.2	2.2	4.15	6.1	10.0	∞	Å

[a]In each column of the table the first line gives the left boundaries of a segment, the second line gives the energy of a segment, and the third line gives the right boundaries of a segment.

dip-to-peak separation match the experimental value. This would require an increase of the well radius by approximately 0.3 Å. Such a match should not actually be expected, since the present theoretical treatment makes no provision for the "Franck-Condon width" [18] contribution. Our current selection of the well size is expected to yield qualitatively correct results. The cross section and its energy derivative are shown in Fig. 5.

Choosing the energy 1.85 eV at the peak of the cross section, we plot in Fig. 6 the "overlap" criterion of Eq. (59) as a function of the r_0 of the QBS function. The maximum is at $r_0=1.6852$ Å, and we use this value for the remainder of the example. Figure 6 actually gives the square of the overlap. At the maximum, the overlap itself is 0.9652, which shows that there is a great deal of similarity between the two functions where they are both defined. For this QBS function, $E_q=10.881$ eV.

Figure 7 shows how the three phase shifts vary with energy in the vicinity of the cross-section peak. We see that the background phase shift is small for the parameters we are using. The actual slope the curve would have if plotted versus k is -0.613 bohr, which is considerably above the Wigner limit of -3.18 bohr corresponding to the radius of the QBS function.

We finish this example now by showing the $\Gamma(E)$ and $\Delta(E)$ functions for the potential. These are given for low energies in Fig. 8. The values at the resonance peak are $\Gamma(E_{res})=1.974$ eV and $\Delta(E_{res})=-9.011$ eV. It is seen that the energy shift is almost constant at this energy and the width function changes little over the width of the resonance. Nevertheless, the dip-to-peak distance of 0.89 eV given above is slightly less than half of the resonance width produced by the FFRP for these parameters. Since the energy shift formula in the form of Eq. (14) involves an integral over all energies, we plot Γ and Δ to higher energies in Fig. 9 as an indication of how such integrals might converge.

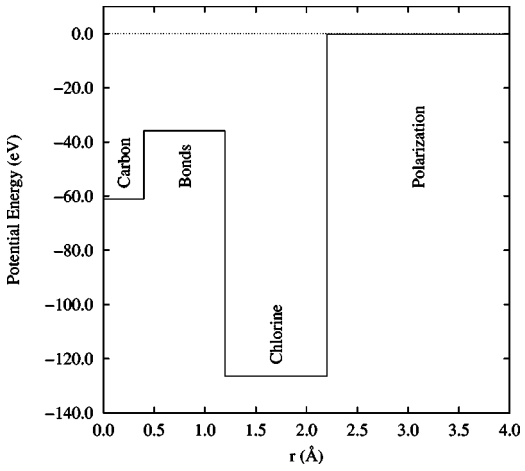

FIG. 12. The inner portion of the potential used for the calculations on CCl_4.

E. More diffuse QBS functions: The dependence upon r_0

During the past 25 years, a number of computational packages for molecular structure calculations have become available. These typically use Gaussian orbital basis sets and typically will carry out *ab initio* Hartree-Fock self-consistent-field calculations for molecules. It has been discovered that the virtual orbital energies from such calculations can be used to guide the assignment of resonances to electronic states of the molecules involving particular antibonding orbitals [19]. Using Koopmans' theorem [20], the virtual orbital energies from these calculations correspond to the E_q quantity we have been calculating.[3] A partly empirical scaling procedure [21] has also been suggested that is designed to compensate for the fact that a $\Delta(E)$ as well as E_q must be known for a successful comparison of theory with experiment for temporary negative ions.

To work, the Hartree-Fock treatments for molecules must be carried out with basis sets that are not too diffuse. When one is dealing with a *stable negative ion*, the standard injunction that "the bigger the basis, the better" certainly stands. With temporary negative ions, however, large basis sets with many diffuse functions merely exhibit variational collapse of the virtual orbital energies, and the corresponding orbitals show little relation to the inner part of the resonant wave function being sought.[4] Unfortunately, over the years a number of studies have appeared in which this error has occurred. In spite of its inappropriateness, such a collapsed energy orbital could still be used in the FFRP, and it is important to see how such overdiffuse functions behave when that procedure is applied. To show this, we have calculated results for this simple well for the four values of r_0: 3.0, 5.0, 7.0, and 9.0 Å. The corresponding values of E_q are 6.68, 2.90, 1.53, and 0.94 eV, respectively. (Compare with the 10.88 eV value above from the optimum r_0.) The resonant and background phase shifts are shown in Fig. 10, and the computed lifetime and energy shift values are in Fig. 11.

[3]As an alternative to using Koopmans' theorem, the total energy of the negative ion may be directly determined.

[4]Another method for dealing with this problem is the stabilization procedure [22,23].

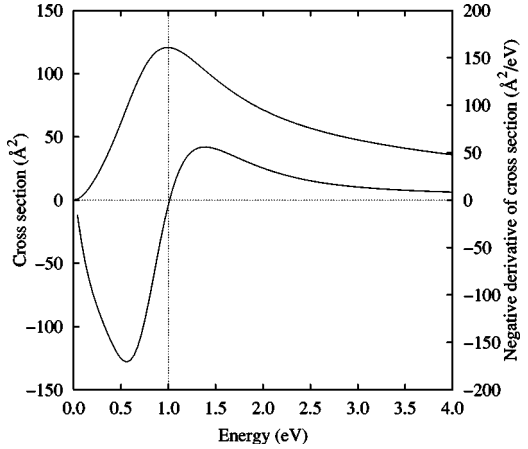

FIG. 13. The cross section in the $l=1$ channel and the negative of its first derivative for CCl_4. A vertical dotted line is drawn at the cross-section maximum.

Using these more diffuse functions causes E_q to decrease, principally because the kinetic energy of the electron is inversely proportional to the square of r_0. At the same time, however, the resonant phase shift deviates more strongly from the total phase shift, and, consequently, the background phase shift becomes larger in magnitude. The $\Gamma(E)$ and $\Delta(E)$ functions also develop much more structure at lower energies as r_0 increases. Except for the behavior of E_q, these other changes are undesirable.

F. A simulated potential for CCl_4

Carbon tetrachloride, CCl_4, is a tetrahedral molecule in its equilibrium geometry and is the closest to spherical of our examples. The equilibrium C—Cl distance is close to 1.8 Å. It has a long-range polarization tail produced by a static polarizability of 75.6 bohr^3 [24]. In this case, we use for our simulated potential one with the seven constant segments given in Table II. The inner portion of the potential is also plotted in Fig. 12.

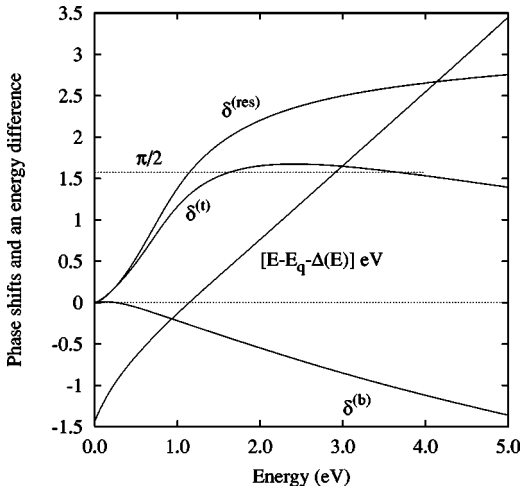

FIG. 14. The phase shifts for the T_2 resonance in CCl_4. The energy difference $E-E_q-\Delta(E)$ is also shown.

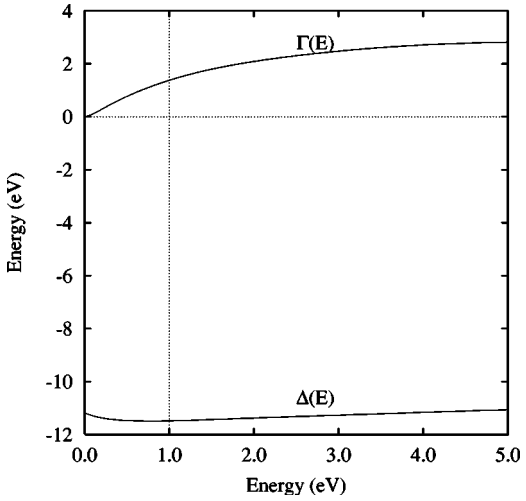

FIG. 15. The graphs of $\Gamma(E)$ and $\Delta(E)$ for the T_2 resonance of CCl_4 at lower energies. A vertical dotted line is drawn at the cross-section maximum.

The outer "surface" of the molecule is set at 2.2 Å. CCl_4 has three T_2 orbitals that are linear combinations of C—Cl bonding orbitals, and ETS measurements have found a shape resonance close to 1.0 eV that has been assigned to the three T_2 combinations of the C—Cl antibonding (σ^*) orbitals. The actual relative values of the inner part of the potential of Table II were based upon a spherical average of the calculated electric potential of CCl_4, but the depths were modified empirically so that there are two triply degenerate bound states of $l=1$ symmetry and a shape resonance with cross section peaking at 1.0 eV. This is consistent with Koopmans' theorem calculations of the T_2 QBS, which show two radial nodes. The bound states represent the T_2 linear combinations of the four C—Cl σ bonding orbitals and four of the nonbonding orbitals on Cl. Figure 13 shows the cross section and its derivative. The dip-to-peak separation is 0.824 eV.

The QBS for the resonance analysis, which in this case must be made orthogonal to the lower states, is arranged to have two radial nodes and terminates at $r_0=2.91$ Å. This

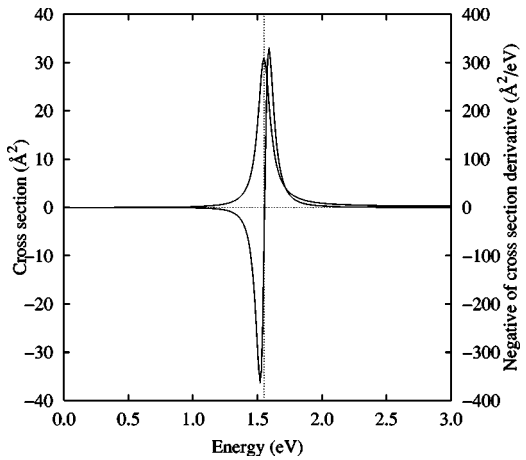

FIG. 16. The cross section and the negative of its first derivative for the $^2B_{1g}$ resonance of C_2H_4. A vertical dotted line is drawn at the cross-section maximum.

TABLE III. Model potential for C_2H_4.

Bond	C	Polarizability tail				
0.0[a]	0.33	1.0	2.5	5.0	10.0	angstrom
−54.29	−73.65	−0.7836	−0.04898	−0.00306	0.0	eV
0.33	1.0	2.5	5.0	10.0	∞	angstrom

[a]See footnote "a" in Table II.

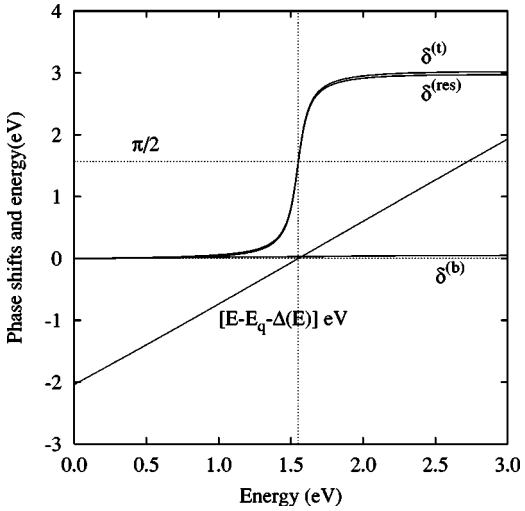

FIG. 17. Various phase shifts and the energy difference $E-E_q-\Delta(E)$ for the $^2B_{1g}$ resonance of C_2H_4 as a function of energy. A vertical dotted line is drawn at the cross-section maximum.

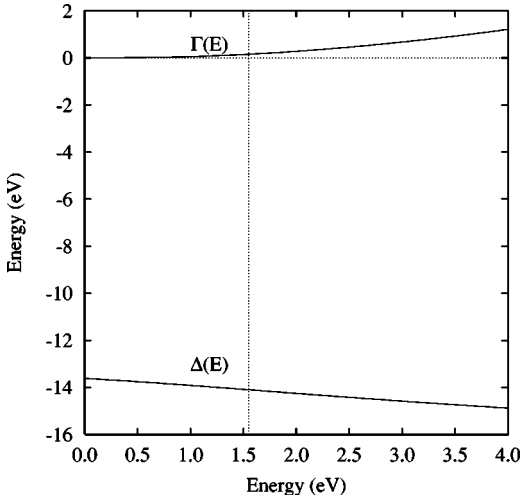

FIG. 18. The $\Gamma(E)$ and $\Delta(E)$ functions for the $^2B_{1g}$ resonance of C_2H_4. A vertical dotted line is drawn at the cross-section maximum.

value maximizes the overlap with the scattering wave function at 1 eV and gives a value of 0.950, which shows a reasonable match. The phase shifts are shown in Fig. 14 along with the quantity $E-E_q-\Delta(E)$. The expectation value of the energy for the projected QBS function is $E_q=12.616$ eV. Figure 15 shows $\Gamma(E)$ and $\Delta(E)$ at lower energies. The behavior of these two functions at high energy is qualitatively the same as that of our previous $l=1$ calculations and, consequently, is not shown.

G. A simulated potential for C_2H_4

Ethylene, C_2H_4, is the simplest of the olefins and has a single low-energy resonance that has been measured by ETS [25]. From the vibrational structure, the 0-0 peak of the resonance was found to be at 1.55 eV and the electronic state has been assigned to a $^2B_{1g}$ symmetry. (see Fig. 16) The leading l value in this case is 2. The C—C internuclear separation is close to 1.34 Å. The segmented potential used is shown in Table III. We include a polarizability tail corresponding to an average polarizability of 28.69 bohr^3 [24]. The potential has been adjusted to give a resonance at the experimental value, and results in a calculated dip-to-peak separation of 0.067 eV. With ETS, the effects of vibration prevent a reliable determination of an experimental separation based purely upon the electronic lifetime.

Following our earlier procedure, we maximized the overlap of the QBS function with the exact wave function at 1.55 eV and obtain a cutoff position of 1.37 Å with an overlap of 0.982 76, which indicates a good match between the functions. For this QBS function, $E_q=15.65$ eV. We show the various phase shifts in Fig. 17. Unlike our earlier $l=1$ calculations, the background phase shift, $\delta^{(b)}$, does not start out in a negative direction immediately at $r=0$, but, rather, it takes on very small positive values at first. For larger values of r, not shown on the graph, it becomes negative and heads toward $-\pi$, as it must.

The values of the lifetime and energy shift functions are shown in Fig. 18. $\Gamma(E)$ is here clearly within its threshold region and $\Delta(E)$ is close to constant over the region around the resonance.

H. Simulated potentials for C_6H_6

We finish with an illustration of a spherical potential with parameters based upon the physical properties of benzene, C_6H_6. Treating benzene as spherical will certainly be more approximate than it was for CCl_4, but at $l=3$ and 4, C_6H_6 has two of the highest l-value shape resonances known. The electron transmission spectrum was determined by Sanche

TABLE IV. Model potential for $^2E_{2u}$ C_6H_6 resonance.

Center	C	Polarizability tail				
0.0[a]	1.1	1.8	3.85	5.9	10.0	Å
0.0	−40.2	−0.32770	−0.05942	−0.00720	0.0	eV
1.1	1.8	3.85	5.9	10.0	∞	Å

[a]See footnote "a" in Table II

and Schulz [26]. The upper *g*-wave resonance is generally believed to be a mixed shape-core excited state, but calculations indicate that a QBS function predominately of the shape sort (≈80%) is reasonable.[5]

1. The $^2E_{2u}$ resonance

In this case, the potential is set to give an *f*-wave resonance around 1 eV, and the values are given in Table IV. Benzene has an average polarizability of 67.5 bohr^3 [24], and a region of the potential is adjusted to reflect this value. Figure 19 shows the cross section and the negative of its derivative. The dip-to-peak separation is only 0.006 eV. Such a small number suggests that the electronic lifetime in the actual molecule probably is also affected by inelastic processes. In addition, the measurements show significant vibrational structure that obscures an estimate of the electronic lifetime.

When we consider the FFRP, we find the optimum QBS function to have an overlap with ψ_l of 0.987 31, which shows a high match. The cutoff radius is 2.35 Å, and the corresponding energy is E_q=6.99 eV. In this case, the background phase shift is very small and is negligible in the range of the resonance. As is the case with C_2H_4, $\delta^{(b)}$ is slightly positive in the neighborhood of 1.0 eV, but it takes on the expected behavior of heading toward $-\pi$ at energies above those on the graph. The various phase shifts are shown in Fig. 20, and the $\Gamma(E)$ and $\Delta(E)$ functions are shown in Fig. 21.

2. The $^2B_{2g}$ resonance

In this case, we set the potential to produce a *g*-wave resonance at the place where a pure shape resonance, unmixed with any core excited component, might hypothetically occur in benzene. It is shown in Table V. The center of the resonance is ≈6.0 eV and the dip-to-peak separation is 0.17 eV. The cross section and the negative of its derivative are shown in Fig. 22.

When we consider the FFRP, we find the optimum QBS function to have an overlap with ψ_l of 0.987 26, which again shows a high match. The cutoff radius is now 2.27 Å, and the corresponding energy is E_q=13.760 eV. The various phase shifts are shown in Fig. 23. Again, the background shows a lower energy region of small positive values before heading to its $-\pi$ destiny. Finally, the values of $\Gamma(E)$ and $\Delta(E)$ for the resonance are shown in Fig. 24. Clearly, even at 6.0 eV and with the relatively large size of the molecule, the $\Gamma(E)$ function is still well in the threshold region.

[5]Unpublished calculations.

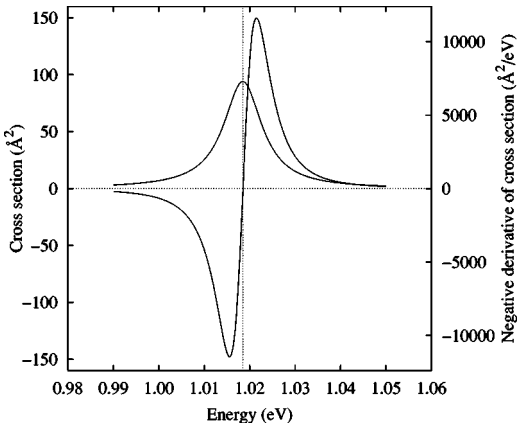

FIG. 19. The cross section and the negative of its first derivative for the $^2E_{2u}$ resonance of C_6H_6. A vertical dotted line is drawn at the cross-section maximum.

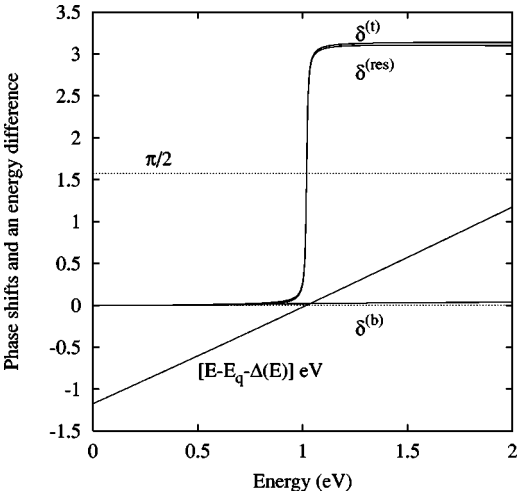

FIG. 20. The phase shifts and the energy difference for the $^2E_{2u}$ resonance of C_6H_6.

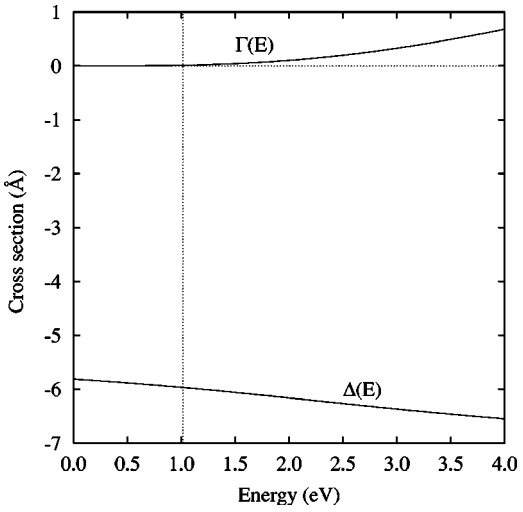

FIG. 21. The width and energy shift functions for the $^2E_{2u}$ resonance of C_6H_6.

TABLE V. Model potential for $^2B_{2g}$ C_6H_6 resonance.

Center	C	Polarizability tail				
0.0[a]	1.1	1.8	3.85	5.9	10.0	Å
−5.0	−51.1	−0.32770	−0.05942	−0.00720	0.0	eV
1.1	1.8	3.85	5.9	10.0	∞	Å

[a]See footnote "a" in Table II.

VI. DISCUSSION

We have illustrated electronic resonant scattering behavior with a number of examples. Although physical data from several actual molecules were used in contriving the potentials, actual comparison with experimental data is precluded by the the fact that our examples treat only elastic scattering in the electronic state, with no effects due to nuclear motion or inelasticity. Nevertheless, several interesting points concerning the behavior of the electronic state have been uncovered.

First we take note of the fact that, for all of the potentials shown here, the value of $\Delta(E)$ is relatively constant in the region up to and past the resonance. Energy shift functions determined for other systems tend to show behavior crossing into the positive region at lower energies [27], where $\Gamma(E)$ functions determined from electronic structure and scattering calculations have been fit empirically to exponential functions. This suggests that our $\Gamma(E)$ functions have, in general, a slower fall-off with higher energies than do those determined from more realistic potentials. (See, particularly, Ref. [13].) At present, we can only conjecture that the step function nature of our potentials may be involved.

The $\Gamma(E)$ function in these examples oscillates through positive values for all energies. It is well known that segmented potentials like those we use can sometimes produce what might be considered spurious oscillatory behavior in quantum-mechanical calculations. With these examples, the oscillations are more the result of the form of the QBS function used here than of the nature of the potentials. As suggested above, a two-segment QBS function can be constructed with a regular Bessel function piece from the origin out to a fixed radius with an exponentially decreasing segment (provided by a modified Bessel function) affixed so that the function is smooth at the breaking point rather than merely continuous. The oscillations in $\Gamma(E)$ occur as much in that case as they do with the sort of function used in the above examples. It is, however, fairly straightforward to show that the oscillations do disappear if functions of the $r^{l+1}\exp(-\alpha r)$ sort are used to represent the QBS functions. Of course, exponential functions are known to be very smooth.

The oscillations are affected only slightly by the sharp breaks in the potentials as seen by their presence in the plane-wave example. The segmented potentials do appear to make the oscillations somewhat irregular at low energies.

In our examples that demonstrate behavior for $l>1$, we find that the background phase shift is quite close to zero at the low energies we have investigated. This fact suggests that higher l values will be easier to deal with in semiempirical considerations, since it is unlikely that background phase shifts must be dealt with. For $l=1$, however, it can be sizable.

We have pointed out that $\delta_l^{(b)}$ for $l>1$ has a substantial region of small positive values at low energy before it becomes negative. Even for CCl_4 and $l=1$, close examination shows that there is a very short region of positive excursion. This disappears when a QBS function is used that is too diffuse. These positive excursions appear to be due to the simulated long-range polarization tail on the potentials. The simple well example of Sec. V D does not show it.

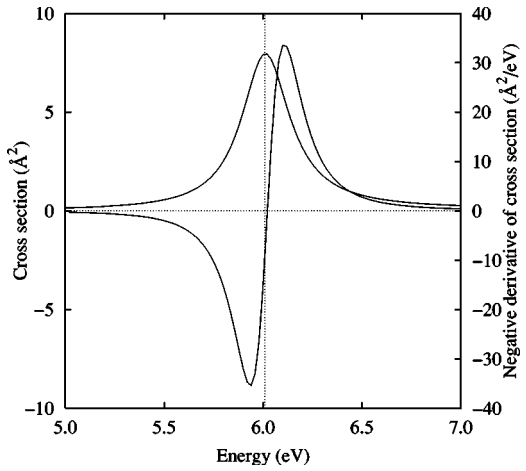

FIG. 22. The cross section and the negative of its first derivative for the $^2B_{2g}$ resonance of C_6H_6. A vertical dotted line is drawn at the cross-section maximum.

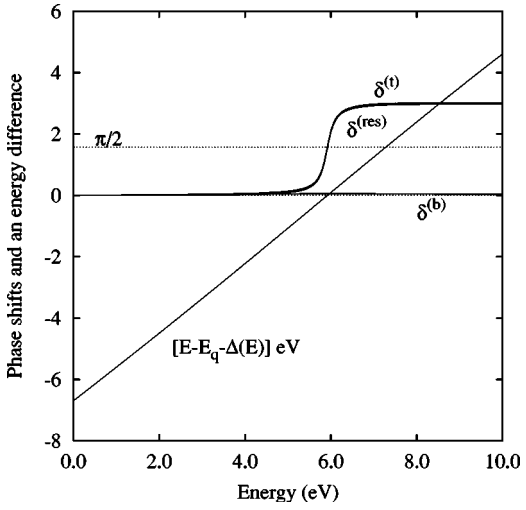

FIG. 23. The phase shifts and the energy difference for the $^2B_{2g}$ resonance of C_6H_6.

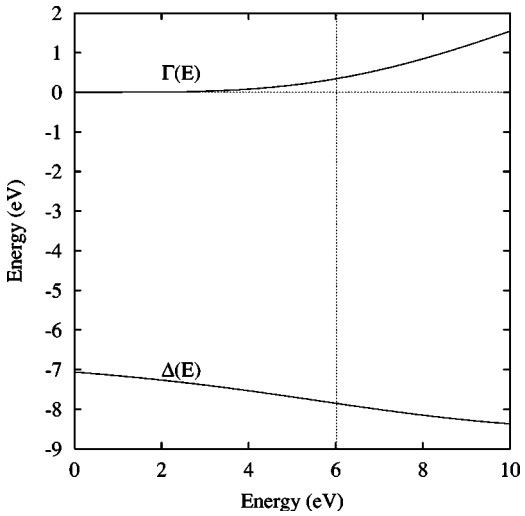

FIG. 24. The width function and the energy shift for the $^2B_{2g}$ resonance of C_6H_6. A vertical dotted line is drawn at the cross-section maximum.

Although the background phase shift can be small, none of our examples indicate that the energy shift is small for the optimum QBS determined using our criterion, and the size of this quantity depends strongly upon the r_0 value taken for $|q\rangle$. In Sec. V E, where we discuss the application to our *t*-butylchloride potential of several QBS functions with larger r_0 values, one sees that several undesirable features develop when using functions that are too diffuse. These include maxima and minima in $\Gamma(E)$ and $\Delta(E)$ as well as resonant phase shifts that are very different from the total phase shift, and background phase shifts that are very different from zero. Therefore, one concludes that the description of resonance processes is likely to be complicated to a considerable extent by using a QBS function that is too diffuse.

It may be noted that the QBS function actually used for CCl_4 has a different character from those of our other calculations, since an orthogonalization to the bound-state functions was required for that system. Thus it is not constrained to be zero for $r > r_0$ as other cases are. Nevertheless, the projected function still has a discontinuous first derivative at r_0, and the qualitative nature of the phase shifts and the $\Gamma(E)$ and $\Delta(E)$ functions is seen to be similar to the results in other cases.

In many molecules, the resonances result from antibonding orbitals that are restricted to a fractional portion of the molecule. These calculations suggest that, in those resonances where there is also a dominant *l* value, there should be relations similar to those shown in Fig. 4 between the dip-to-peak separation and the size of that portion of the molecule supporting the potential that gives the resonance. Many resonances, however, are not expected to have dominant *l* values.

Finally, we make a more mathematical observation. Returning to Eq. (41), the root of the matrix element, $\langle q|G_0(E)|q\rangle$, has an interesting interpretation if we use the spectral representation of the Green's function,

$$G_0(E) = \int_0^\infty \frac{2|\psi^{(t)}\rangle\langle\psi^{(t)}|dE'}{\pi k(E-E')}, \tag{61}$$

$$\langle q|G_0(E)|q\rangle = \int_0^\infty \frac{2|\langle b|\psi^{(t)}\rangle|^2 dE'}{\pi k(E-E')}. \tag{62}$$

Thus the square of the overlap divided by *k* and weighted by the reciprocal of $E-E'$ may be thought to have equal areas on either side of E_{res}, with, however, the correct recognition of the fact that the integral is the Cauchy principal value of the integrand.

ACKNOWLEDGMENTS

The author wishes to thank P. D. Burrow and I. I. Fabrikant for many useful conversations concerning this work.

[1] H. Feshbach, Ann. Phys. (N.Y.) **5**, 357 (1958).
[2] U. Fano, Phys. Rev. **124**, 1866 (1961).
[3] H. Feshbach, Ann. Phys. (N.Y.) **19**, 287 (1962).
[4] H. Feshbach, Ann. Phys. (N.Y.) **43**, 410 (1967).
[5] G. A. Parker, J. C. Light, and B. R. Johnson, Chem. Phys. Lett. **73**, 572 (1980).
[6] H. M. Nussenzveig, Nucl. Phys. **11**, 499 (1959).
[7] K. W. McVoy, in *Fundamentals in Nuclear Theory*, edited by A. de Shalit and C. Villi (International Atomic Energy Agency, Vienna, 1967).
[8] J. R. Taylor, *Scattering Theory* (John Wiley & Sons, Inc., New York, 1972).
[9] R. K. Nesbet, Phys. Rev. A **24**, 1184 (1981).
[10] W. Domcke, Phys. Rev. A **28**, 2777 (1983).
[11] J. N. Bardsley, J. Phys. B **1**, 349 (1968).
[12] R. K. Nesbet, *Variational Methods in Electron-atom Scattering Theory* (Plenum Press, New York, 1980).
[13] M. Berman, C. Mündel, and W. Domcke, Phys. Rev. A **31**, 641 (1985).
[14] M. Abramowitz and I. A. Stegun, *Handbook of Mathematical Functions* (National Bureau of Standards, U. S. Government Printing Office, Washington, D. C., 1970).
[15] E. P. Wigner, Phys. Rev. **98**, 145 (1955).
[16] L. Sanche and G. J. Schulz, Phys. Rev. Lett. **26**, 943 (1971).
[17] K. Aflatooni, G. A. Gallup, and P. D. Burrow, J. Phys. Chem. **104**, 7359 (2000).
[18] F. H. Mies, Phys. Rev. **175**, 164 (1968).
[19] K. D. Jordan and P. D. Burrow, Chem. Rev. (Washington, D.C.) (Washington, D.C.) **87**, 557 (1987).
[20] T. A. Koopmans, Physica (Amsterdam) **1**, 104 (1934).
[21] D. Chen and G. A. Gallup, J. Chem. Phys. **93**, 8893 (1990).
[22] H. S. Taylor, Adv. Chem. Phys. **18**, 19 (1970).
[23] A. U. Hazi and H. S. Taylor, Phys. Rev. A **1**, 1109 (1970).
[24] *CRC Handbook of Chemistry and Physics*, 84th ed., edited by D. R. Lide, (CRC Press, Boca Raton, FL, 2003).
[25] P. D. Burrow and K. D. Jordan, Chem. Phys. Lett. **36**, 594 (1975).
[26] L. Sanche and G. J. Schulz, J. Chem. Phys. **58**, 479 (1973).
[27] W. Domcke, Phys. Rep. **208**, 97 (1991).